Article for Special issue: Molecular Profiling in Lung Cancer

Identification of a clinically relevant signature for early progression in KRAS-driven Lung Adenocarcinoma

Sarah Neidler[1], Björn Kruspig[1], Kay Hewit[2], Tiziana Monteverde[1], Katarina Gyuraszova[1], Attila Braun[3,4], William Clark[2], Daniel James[2], Ann Hedley[2], Bernhard Nieswandt[3], Emma Shanks[2], Craig Dick[5] & Daniel J. Murphy[1,2]*

[1] Institute of Cancer Sciences, University of Glasgow, Glasgow G61 1QH, United Kingdom.
sarahneidler@gmx.de; Bjorn.Kruspig@glasgow.ac.uk; tiziana.monteverde@manchester.ac.uk; Katarina.Gyuraszova@glasgow.ac.uk; Daniel.murphy@glasgow.ac.uk

[2] CRUK Beatson Institute, Garscube Estate, Glasgow G61 1BD, United Kingdom.
kay.hewit@glasgow.ac.uk; w.clark@beatson.gla.ac.uk; d.james@beatson.gla.ac.uk; a.hedley@beatson.gla.ac.uk; e.shanks@beatson.gla.ac.uk

[3] Institute of Experimental Biomedicine, University Hospital Wuerzburg, DE 97080, Germany.
Attila.braun@virchow.uni-wuerzburg.de

[4] Rudolf Virchow Center, Julius Maxmilians University of Wuerzburg, DE97080, Germany.
Bernhard.nieswandt@virchow.uni-wuerzburg.de

[5] Queen Elizabeth University Hospital, Glasgow, G51 4TF, United Kingdom.
Craig.Dick@ggc.scot.nhs.uk

* Corresponding author
Daniel.murphy@glasgow.ac.uk
+44 141 330 8710

Abstract

Inducible genetically defined mouse models of cancer uniquely facilitate the investigation of early events in cancer progression, however there are valid concerns about the ability of such models to faithfully recapitulate human disease. We developed an inducible mouse model of progressive lung adenocarcinoma (LuAd) that combines sporadic activation of oncogenic $KRas^{G12D}$ with modest overexpression of c-MYC (KM model). Histological examination revealed a highly reproducible transition from adenoma to locally invasive adenocarcinoma within 6 weeks of oncogene activation. Laser-capture microdissection coupled with RNA-SEQ was employed to determine transcriptional changes associated with tumour progression. Upregulated genes were triaged for relevance to human LuAd using datasets from Oncomine and cBioportal. Selected genes were validated by RNAi screening in human lung cancer cell lines and examined for association with lung cancer patient overall survival using KMplot.com. Depletion of progression-associated genes resulted in pronounced viability and/or cell migration defects in human lung cancer cells. Progression-associated genes moreover exhibited strong associations with overall survival, specifically in human lung adenocarcinoma, but not in squamous cell carcinoma. The KM mouse model faithfully

recapitulates key molecular events in human lung cancer and is a useful tool for mechanistic interrogation of LuAd progression.

Keywords: Lung Adenocarcinoma; KRAS; MYC; ERBB; Mouse models of cancer; RNA-SEQ

1. Introduction

Genetically engineered mouse models (GEMMs) are powerful tools for understanding the roles of specific oncogenes and tumour suppressors in cancer development and progression. The term "GEMM" spans a broad spectrum of design strategies, ranging from constitutive whole-body deletion of tumour suppressors or overexpression of oncogenes from tissue-specific promoter fragments, the latter typically resulting in artificially high levels of oncogene expression in every cell of a given tissue, to more refined conditional allelic models that allow for sporadic activation/deletion of the target allele in a temporally controlled manner [1, 2]. For even the most elegantly designed GEMMs however, there are valid concerns about the ability of such models to faithfully recapitulate the molecular evolution and features of human cancer [3]. This is particularly true for cancers such as lung cancer that arise primarily from exposure to environmental toxins. Given that GEMMs are increasingly used for pre-clinical testing of novel treatment strategies it is vitally important to interrogate their suitability for this role [4].

Development of the lsl-KRas^{G12D} allele, in which a single-nucleotide altered coding exon of KRas was inserted into the endogenous KRas locus downstream of a CRE-deletable lox-stop-lox cassette, represented a watershed moment in the progress of GEMM development [5]. Aside from the requirement for exposure to CRE recombinase, expression of this allele is entirely physiological, marking a major departure from previous transgenic models that typically relied on pronounced overexpression of oncogenes from strong tissue-restricted promoters [6]. An oncogene that is overexpressed as well as mutated will elicit a much stronger signal than one that is merely mutated, with profound implications for phenotypic evolution [7]. Given that KRAS is much more frequently mutated without overexpression than with [8], the lsl-KRas^{G12D} allele better reflects the expression of activated KRAS in human disease than would an overt overexpression allele. Perhaps unsurprisingly, this allele emerged to be relatively inefficient in driving late stage cancer but very effective in driving incipient early stage disease [5]. The modest oncogenic output of lsl-KRas^{G12D} however turns out to be its principle strength, allowing for the investigation of spontaneous tumour progression from pre-cancerous lesions. Accordingly, combination of this allele with additional oncogenes or tumour suppressors readily drives progression of incipient tumours [9-11].

By comparison, modeling the oncogenic output of MYC deregulation at a level that reflects incipient human cancer is more challenging. Although MYC expression is typically quite high in late-stage human cancers, pronounced overexpression of MYC in normal tissue immediately elicits an apoptotic response, eliminating the offending cells [12-14]. The prior or simultaneously inactivation of apoptosis is typically a prerequisite for tumour initiation by high levels of MYC [15, 16]. Insertion of a conditional and acutely inducible allele of c-MYC into the Rosa26 locus led to the serendipitous discovery of a level of MYC expression below the threshold required to drive apoptosis [17]: Rosa26-lsl-MycER^{Tam} mice express a Tamoxifen-dependent allele of the c-MYC oncogene fused in-frame to a minimal ligand-binding domain of human estrogen receptor, the latter modified to

prevent activation by circulating estrogen [18]. Functional characterization of this allele demonstrated expression of MycER^{Tam} in the near-physiological range, relative to endogenously expressed c-Myc. Importantly, this level of expression sufficed to drive ectopic proliferation in all adult organs examined, without triggering widespread MYC-dependent apoptosis [17]. The implication of this observation is that modest MYC overexpression may, by virtue of evading intrinsic tumour suppression, exhibit enhanced tumour promoting activity compared with higher levels that overtly trigger apoptosis [19, 20]. The sustained activity of MycER^{Tam} however requires continuous administration of the synthetic ligand Tamoxifen, which exerts both agonist and antagonist activity on cells expressing the endogenous estrogen receptor, potentially impacting on MYC-driven phenotypes [21]. We therefor re-engineered the allele without the ER moiety to retain the low level of expression afforded by the Rosa26 locus and the CRE-dependence of expression, but to liberate MYC's transcriptional activity from dependence upon Tamoxifen (Fig. S1).

2. Results

2.1 MYC accelerates KRas^{G12D}-driven LuAd development

Analysis of the TCGA pan-cancer cohort of Lung Adenocarcinoma (LuAd) revealed amplification and/or overexpression of *c-MYC* in up to 20% of LuAd and a significant enrichment for *MYC* overexpression in *KRAS* mutant tumours (p=0.025) (Figure 1A). We used replication defective recombinant Adenoviral delivery of CRE recombinase (Ad-CRE), administered by intranasal inhalation, to sporadically activate expression of transgenic MYC in the lungs of heterozygous Rosa26$^{DM.lsl\text{-}MYC/+}$ (M) and homozygous Rosa26$^{DM.lsl\text{-}MYC/lsl\text{-}MYC}$ (M^2) mice. Acute ectopic proliferation of airway epithelium, detected by BrdU incorporation 3 days after allele activation, was only detectable in homozygous mice (Fig. 1B). No tumours could be detected in Ad-CRE induced M or M^2 mice housed for up to 1 year after induction (data not shown). We therefore asked if Rosa26-driven MYC could cooperate with endogenously expressed active KRas to accelerate lung tumour development. Comparison of lung tumour burden in Ad-Cre induced lsl-KRas$^{G12D/+}$ (K), lsl-KRas$^{G12D/+}$;Rosa26$^{DM.lsl\text{-}MYC/+}$ (KM), and lsl-KRas$^{G12D/+}$;Rosa26$^{DM.lsl\text{-}MYC/lsl\text{-}MYC}$ (KM^2), mice at 6 weeks post induction (PI) revealed a dramatic, MYC-dose dependent, increase in the percentage of lung area occupied by tumours (Fig. 1C). Histopathological analysis of KM^2 tumours at 2, 4 and 6 weeks showed uniform progression of all incipient KM^2 tumours to low-grade Adenocarcinoma in situ (Fig. 1D). This contrasts with KRas$^{G12D/+}$-only lesions that fail to progress beyond atypical adenomatous hyperplasia within this time (Fig. 1E) [5].

2.2 A transcriptomic signature of KRAS LuAd tumour progression

As we recently reported [22], KM^2 tumours sporadically progress to higher-grade disease characterized by increased morphologic heterogeneity and sharply increased phosphorylation of Erk1/2, downstream of KRAS. We used laser-capture microdissection to collect such p-Erk^{HI} tumour regions, along with matching p-Erk^{LO} regions from the same tumours, and RNA-SEQ analysis to determine changes in gene expression associated with progression of KM^2 LuAd [22]. Across tumours from 4 mice we detected 1396 genes with significantly altered expression. To establish an expression signature relevant for human cancer, we used an arbitrary cutoff of 2.5X increased expression and evidence of overexpression and/or amplification from human LuAd datasets [23-25]

available via Oncomine and cBioportal to stratify significantly upregulated genes, yielding a list of 51 genes (Table 1). This list notably includes ERBB-family ligands *Ereg* and *Areg*, Wnt pathway constituents *Sox9* and *Porcn*, nutrient transporters *Slc2a1* and *Slc38a1*, and glycolytic enzymes *Gapdh* and *Pgk1*, the latter 4 suggestive of increased metabolic demand during LuAd progression.

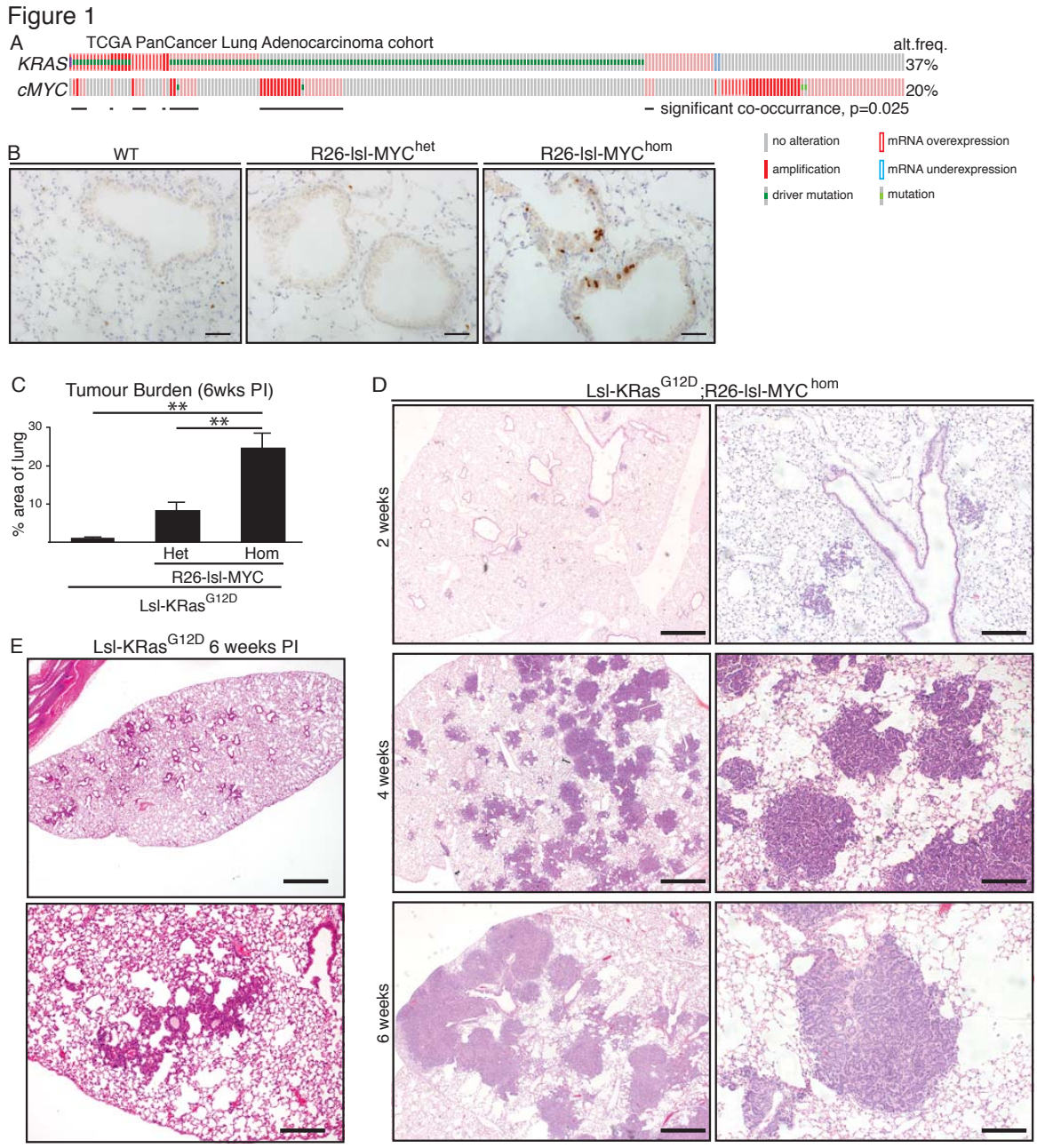

Figure 1: MYC accelerates KRas^{G12D}-driven LuAd development

A) *Frequency of mutation, copy number and mRNA expression alteration of KRAS and cMYC in the TCGA Pan Cancer lung Adenocarcinoma cohort, accessed through cBioportal. For mRNA analysis, Z score threshold was set to 1.5. Horizontal black lines indicate cases with alteration of both KRAS and MYC.* ***B)*** *Ectopic proliferation induced by CRE-dependent activation of Rosa26-lsl-MYC in airway epithelium evidenced by BrdU incorporation. Images are representative of at least 4 mice/genotype. Scale bar = 40μm.* ***C)*** *Overall tumor burden, defined as the percent of lung area occupied by tumor tissue, in mice bearing 1 (N= 9) or 2 (N=11) R26-lsl-MYC combined with lsl-KRas^{G12D}, compared with lsl-KRas^{G12D} alone (N=6), measured 6 weeks PI. Mean ± SEM shown. ** deontes p<0.01 (T-test).* ***D)*** *Adult mice (8-10wks old) bearing the*

Preprints (www.preprints.org) | NOT PEER-REVIEWED | Posted: 30 March 2019 doi:10.20944/preprints201903.0286.v1

Peer-reviewed version available at Cancers 2019, 11, 600; doi:10.3390/cancers11050600

indicated conditional alleles were administered 1x10^7 pfu Adeno-CRE by intranasal installation and harvested at the indicated times post infection (PI). Micrographs show representative H&E-stained lung tissue. Scale bars = 1mm (left panels) and 200μm (right panels). ***E)*** *Age matched lsl-KRas^{G12D} mice were induced with the same pfu Adeno-CRE as (D) and tumour burden examined after 6 weeks. Scale bars = 1mm (top panel) and 200μm (bottom panel).*

Table 1: RNA-SEQ analysis of p-ERK-associated KM lung tumour progression

Entrez ID	Symbol	Gene Name	RNA- SEQ Lo-Hi Read Count p-ERK neg	RNA- SEQ Lo-Hi Read Count p-ERK pos	Mean FC	FDR	Amplified in hu NSCLC cBioportal	Overexpressed hu NSCLC Oncomine
13874	**Ereg**	epiregulin	5 - 39	227 - 376	**24.82**	2.78E-13	Y	Y
20682	**Sox9**	SRY-box containing gene 9	6 - 31	39 - 330	**15.79**	7.48E-04	Y	Y
13386	**Dlk1**	delta-like 1 homolog (Drosophila)	63 - 400	341 - 2114	**10.46**	2.33E-26	Y (SCC)	N
56386	**B4galt6**	UDP-Gal:betaGlcNAc beta 1,4-galactosyltransferase, polypeptide 6	7 - 91	113 - 491	**9.46**	1.24E-03	Y (SCC)	Y
70350	**Basp1**	brain abundant, membrane attached signal protein 1	0 - 66	89 - 307	**9.03**	1.31E-04	Y >10%	Y
16398	**Itga2**	integrin alpha 2	49 - 185	185 - 1239	**6.79**	2.47E-11	<1%	Y
12740	**Cldn4**	claudin 4	7 - 49	64 - 117	**6.11**	1.16E-02	Y	Y
12484	**Cd24a**	CD24a antigen	145 -1040	1411 - 1580	**5.94**	1.40E-15	No Data	Y
105727	**Slc38a1**	solute carrier family 38, member 1	60 - 153	248 - 716	**5.68**	1.17E-11	Y	Y
272322	**Arntl2**	aryl hydrocarbon receptor nuclear translocator-like 2	15 - 59	44 - 156	**4.54**	4.90E-02	Y >7%	Y
13506	**Dsc2**	desmocollin 2	14 - 148	62 - 302	**4.43**	4.51E-02	Y (SCC)	Y
11839	**Areg**	amphiregulin	156 - 234	526 - 831	**4.25**	4.98E-11	Y	Y
20200	**S100a6**	S100 calcium binding protein A6 (calcyclin)	115 - 215	234 - 1017	**4.00**	1.51E-07	Y >14%	Y
192897	**Itgb4**	integrin beta 4	31 - 89	81 - 310	**3.92**	2.29E-02	Y	Y
224079	**Atp13a4**	ATPase type 13A4	242 - 399	711 - 1002	**3.92**	3.03E-14	Y >25% SCC	Y
71819	**Kif23**	kinesin family member 23	151 - 359	313 - 994	**3.76**	8.81E-07	<1%	Y
53627	**Porcn**	porcupine homolog (Drosophila)	38 - 52	76 - 182	**3.59**	4.85E-03	<1%	N
16691	**Krt8**	keratin 8	67 - 380	489 - 699	**3.57**	1.87E-05	Y	Y
22329	**Vcam1**	vascular cell adhesion molecule 1	11 - 133	75 - 442	**3.57**	3.59E-02	<1%	N
16668	**Krt18**	keratin 18	503 - 827	1192 - 1850	**3.50**	1.80E-11	Y	Y
16782	**Lamc2**	laminin, gamma 2	457 - 677	1104 - 1825	**3.48**	2.56E-09	Y >7%	Y
27279	**Tnfrsf12a**	tumor necrosis factor receptor superfamily, member 12a	30 - 54	86 - 135	**3.42**	1.47E-02	Y	Y
216350	**Tspan8**	tetraspanin 8	329 - 570	635 - 1848	**3.41**	5.23E-06	Y >5%	Y
338375	**Atp6v1g3**	ATPase, H+ transporting, lysosomal V1 subunit G3	46 - 94	91 - 232	**3.40**	2.80E-03	Y >7%	N
13601	**Ecm1**	extracellular matrix protein 1	44 - 79	100 - 173	**3.25**	7.13E-03	Y >16%	Y
66166	**S100a14**	S100 calcium binding protein A14	89 - 210	218 - 530	**3.18**	6.52E-04	Y >14%	Y
19039	**Lgals3bp**	lectin, galactoside-binding, soluble, 3 binding protein	178 - 333	472 - 679	**3.16**	2.09E-07	Y	Y
23959	**Nt5e**	5' nucleotidase, ecto	148 - 339	462 - 697	**3.04**	1.20E-05	Y (SCC)	Y
16763	**Lad1**	ladinin	141 - 344	401 - 619	**3.01**	2.92E-05	Y >7%	Y
16011	**Igfbp5**	insulin-like growth factor binding protein 5	296 - 422	414 - 1197	**2.99**	1.36E-05	<1%	Y
12304	**Pdia4**	protein disulfide isomerase associated 4	966 - 1887	2519 - 3183	**2.98**	3.16E-05	Y	Y
12494	**Cd38**	CD38 antigen	37 - 64	77 - 167	**2.97**	3.82E-02	<1%	Y
16669	**Krt19**	keratin 19	203 - 469	664 - 969	**2.96**	2.06E-06	<1%	Y
20525	**Slc2a1**	solute carrier family 2 (facilitated glucose transporter), member 1	57 - 114	125 - 249	**2.95**	1.11E-02	Y	Y
225908	**Myrf**	myelin regulatory factor	57 - 163	95 - 474	**2.92**	1.26E-02	<1%	Y
240753	**Plekha6**	pleckstrin homology domain containing, family A member 6	185 - 353	490 - 692	**2.91**	3.34E-05	<1%	Y
17988	**Ndrg1**	N-myc downstream regulated gene 1	77 - 333	208 - 716	**2.84**	7.71E-03	Y >5%	Y
29809	**Rabgap1l**	RAB GTPase activating protein 1-like	1211 - 1754	2578 - 4099	**2.83**	3.95E-05	Y >8%	N
21664	**Phlda1**	pleckstrin homology-like domain, family A, member 1	105 - 226	175 - 402	**2.82**	7.01E-04	<1%	Y
14433	**Gapdh**	glyceraldehyde-3-phosphate dehydrogenase	79 - 106	136 - 216	**2.80**	1.08E-02	Y (SCC)	Y
16592	**Fabp5**	fatty acid binding protein 5, epidermal	78 - 175	115 - 410	**2.79**	6.15E-03	Y	Y
12764	**Cmas**	cytidine monophospho-N-acetylneuraminic acid synthetase	49 - 106	108 - 283	**2.75**	4.21E-02	Y>5%	Y
105348	**Golm1**	golgi membrane protein 1	509 - 1420	1343 - 2171	**2.75**	3.84E-05	N	Y
64292	**Ptges**	prostaglandin E synthase	59 - 154	158 - 286	**2.73**	5.26E-03	Y	Y
53416	**Stk39**	serine/threonine kinase 39	304 - 659	872 - 1127	**2.71**	2.21E-06	Y	Y
27999	**Fam3c**	family with sequence similarity 3, member C	351 - 642	673 - 1078	**2.65**	6.40E-09	Y	N
18655	**Pgk1**	phosphoglycerate kinase 1	138 - 178	220 - 425	**2.61**	1.23E-03	<1%	Y
12297	**Cacnb3**	calcium channel, voltage-dependent, beta 3 subunit	56 - 87	78 - 147	**2.59**	3.70E-02	Y	N
94185	**Tnfrsf21**	tumor necrosis factor receptor superfamily, member 21	121 - 238	232 - 348	**2.57**	1.58E-03	Y	Y
14261	**Fmo1**	flavin containing monooxygenase 1	174 - 256	186 - 1098	**2.57**	7.51E-03	Y >7%	Y
20195	**S100a11**	S100 calcium binding protein A11 (calgizzarin)	245 - 696	594 - 1252	**2.53**	1.21E-04	Y >15%	Y
26365	**Ceacam1**	carcinoembryonic antigen-related cell adhesion molecule 1	326 - 608	648 - 1286	**2.50**	1.08E-05	Y	Y

Table 1: Specific genes upregulated in pErk^{High} KM tumour regions

Genes were selected based on evidence of overexpression and/or amplification in human NSCLC. Range of RNA-SEQ read count values, normalised for total reads per sample, for the indicated genes. FC = fold change. FDR = false discovery rate. For "Amplified in human NSCLC": Y = yes (1-5%) with >5% and <1% where noted; N = No; SCC = squamous Cell Carcinoma where noted, otherwise Adenocarcinoma or unclassified. For "Overexpressed in human NSCLC": Y = Yes; N = No.

2.3 Functional validation of p-Erk associated genes: Contribution to cell propagation

We assembled a focused library of 4 separate siRNAs targeting each of the 51 p-Erk^{HI}-associated genes implicated in human non-small cell lung cancer (NSCLC) and confirmed the efficacy of targeted depletion of a randomly chosen subset in A549 cells using Q-PCR (Figure S2A). We then screened the effect of each siRNA individually for the ability to suppress propagation of 3 KRAS-

Preprints (www.preprints.org) | NOT PEER-REVIEWED | Posted: 30 March 2019 doi:10.20944/preprints201903.0286.v1

Peer-reviewed version available at Cancers 2019, 11, 600; doi:10.3390/cancers11050600

mutated human NSCLC cell lines, A549, H2009 and H460. Cells were reverse transfected with individual siRNAs at low density and allowed to propagate for up to 72 hrs, whereupon cell numbers were measured by high-content microscopy. Each screen included positive (Allstars, Qiagen) and negative (non-targeting siRNA) controls. The effect of each individual siRNA on cell propagation was calculated as percent suppression of viability (SoV), relative to non-targeting siRNA-transfected cells, in each of the 3 cell lines. The mean SoV of all siRNAs across the entire dataset (M) was calculated for each cell line and used to set a threshold for acceptance or rejection of the effects of individual siRNAs: siRNAs that resulted in SoV > M were thus scored "positive". Figure 2A summarizes the results of this analysis: siRNAs yielding greater than average SoV in all 3 cell lines are indicated by red bars; those that scored positive in 2/3 cell lines by yellow bars. Thus, for each *FMO1*, *KIF23*, *KRT19* and *SLC2A1*, the same 3 out of 4 siRNAs consistently suppressed cell propagation in all three human NSCLC lines tested (Fig. 2B) allowing us to say with confidence that these 4 genes are required to sustain proliferation of KRAS mutant human NSCLC cells. The functional requirement of nascent lung tumours for Kif23 has moreover been verified in vivo [26].

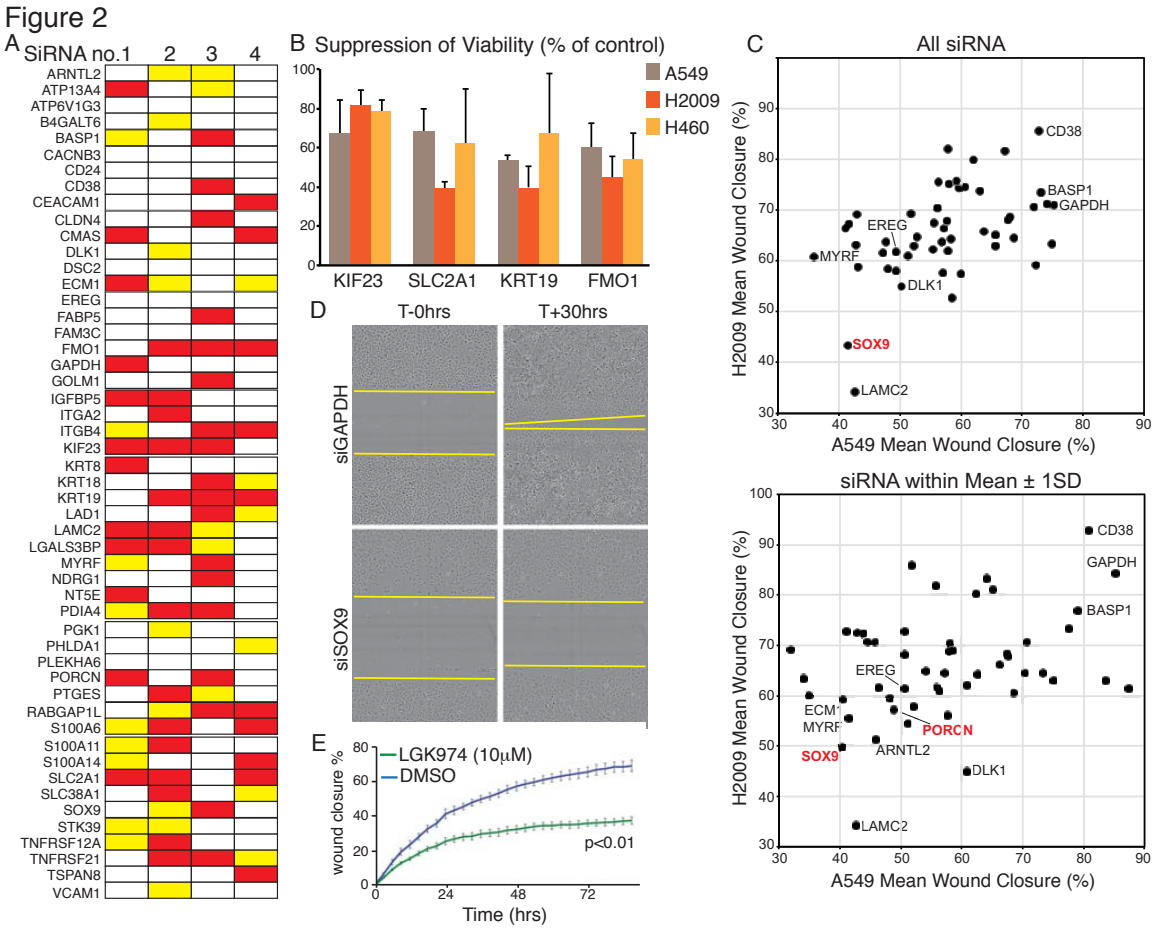

Figure 2: Validation of KM tumour progression signature genes in human cell lines

A) *Summary of suppression of viability (SoV) screening data using 4 individual siRNAs to target each indicated gene in A549, H460 and H2009 cells. Red bars indicate greater than average SoV in all 3 cell lines; Yellow bars indicate greater than average SoV in 2/3 lines.* ***B)*** *Mean (±SD) SoV of 3 siRNAs, targeting each of the indicated transcripts, that exhibit consistent effects in all three cell lines.* ***C)*** *Suppression of H2009 (y-axis) and A549 (x-axis) cell migration upon depletion of gene products listed in (A). Top panel: Mean distance*

migrated (defined as percent "wound" closure) after separate transfection with 4 siRNAs targeting each gene. Lower panel: Mean migration distance values for siRNAs falling within 1 standard deviation of the mean of all 4 for each targeted gene. ***D)*** *Representative photomicrographs showing suppression of cell migration upon depletion of Wnt pathway component SOX9. Compare with GAPDH (top panels).* ***E)*** *Pharmacological suppression of Wnt signaling using the PORCN inhibitor LGK974 suppresses migration of A549 cells, as determined by Incucyte time-lapse microscopy. Error bars show SD of technical triplicates. P value from T-Test shown. All data are representative of 3 or more experiments.*

2.4 Functional validation of p-Erk associated genes: WNT signaling contributes to cell motility.

Given the association of the dataset with an invasive phenotype [22] we used our focused siRNA library to ask if any of the selected genes affect migration of human NSCLC cells. RNAi reverse transfected A549 or H2009 cells were seeded in 96-well plates and grown to confluency over 48hrs. Monolayers were then scratch 'wounded' with a woundmaker tool and monitored by Incucyte time-lapse video microscopy until the scratch wounds of control siRNA-transfected cells were circa 90% closed. Total cell number per well was determined at the end of each experiment to assess the potential influence of loss of viability (LoV) upon the migration assay. The mean wound closure and LoV values were determined for each siRNA and averaged across all 4 siRNAs for each gene. Figure S2B shows the mean migration data plotted against the mean LoV for each gene for A549 and H2009 cells (H460 cells were omitted from this analysis as they failed to migrate under the conditions tested). Only in the case of KIF23 depletion was LoV found to consistently account for the observed suppression of scratch wound closure. Depletion of LAMC2, previously validated as required for invasion and metastasis in NSCLC [27], consistently suppressed migration in both cell lines. Interestingly, depletion of WNT signaling components, SOX9 or PORCN [28], also suppressed migration in both cell lines (Fig 2C, D), suggesting that WNT signaling contributes to NSCLC tumor progression beyond its ability to suppress senescence [29-31]. This effect was confirmed in A549 cells by pharmacological inhibition of PORCN (Figure 2E).

2.5 Relevance of the murine dataset for human pulmonary Adenocarcinoma

We used an online Kaplan Meier meta-analysis tool [26] to investigate the association of each of the 51 selected genes with overall survival (OS) and responsiveness to radio- or chemotherapy among human lung cancer patients. Cox regression plots of patient survival were generated based on a median split of gene expression levels above (High) or below (Low) median gene expression. Differential expression of 33 of the 51 genes is associated with significantly altered OS across all lung cancers (N=1926), with high expression of 25 genes associated with significantly decreased OS (logrank $p<0.05$). Upon analysis of histological subtypes, 35 genes are associated with significantly altered OS of Adenocarcinoma patients (N=719), with 28 genes overlapping with those significantly altered across all lung tumors. In contrast, only 3 genes (*KRT8, KRT18* and *GAPDH*) correlate with significantly reduced OS of Squamous Cell Carcinoma patients (N=525), mirroring the histological classification of the murine KM tumors as Adenocarcinoma (Fig. 3A). Strikingly, high expression of *SLC2A1*, encoding the glucose transporter GLUT1, and the glycolytic genes *GAPDH* & *PGK1*, were associated with strongly reduced OS, particularly in the Adenocarcinoma subtype (Fig. 3B), consistent with the prognostic value of FDG-PET in LuAd [27].

Across all lung cancers, high expression of 5 of the 51 genes is associated with significantly worse outcome in patients that received chemotherapy (N=176): *SLC2A1, S100A11, GAPDH, FABP5* and *ARNTL2*. The latter 2 are also associated with worse outcome in patients that received radiotherapy (N=70), with hazard ratios of 2.34 and 3.25, respectively. High expression of a further 4 genes is also associated with poorer response to radiotherapy: *S100A14, PHLDA1, EREG* and *CD24* (HRs ranging from 1.89-1.93). In contrast, high *IGFBP5* expression is associated with better outcome in patients that received radiotherapy (HR = 0.56) while high *CEACAM1* expression is associated with better outcome in patients that received chemotherapy (HR = 0.57). Expression of ERBB ligands *EREG* and *AREG* previously led us to identify an unexpected requirement for signaling through the ERBB family of receptor tyrosine kinases for development, progression and maintenance of KRAS driven LuAd, verified independently by a second group [22, 28]. Notably, high expression of either *ERBB2* or

Figure 3

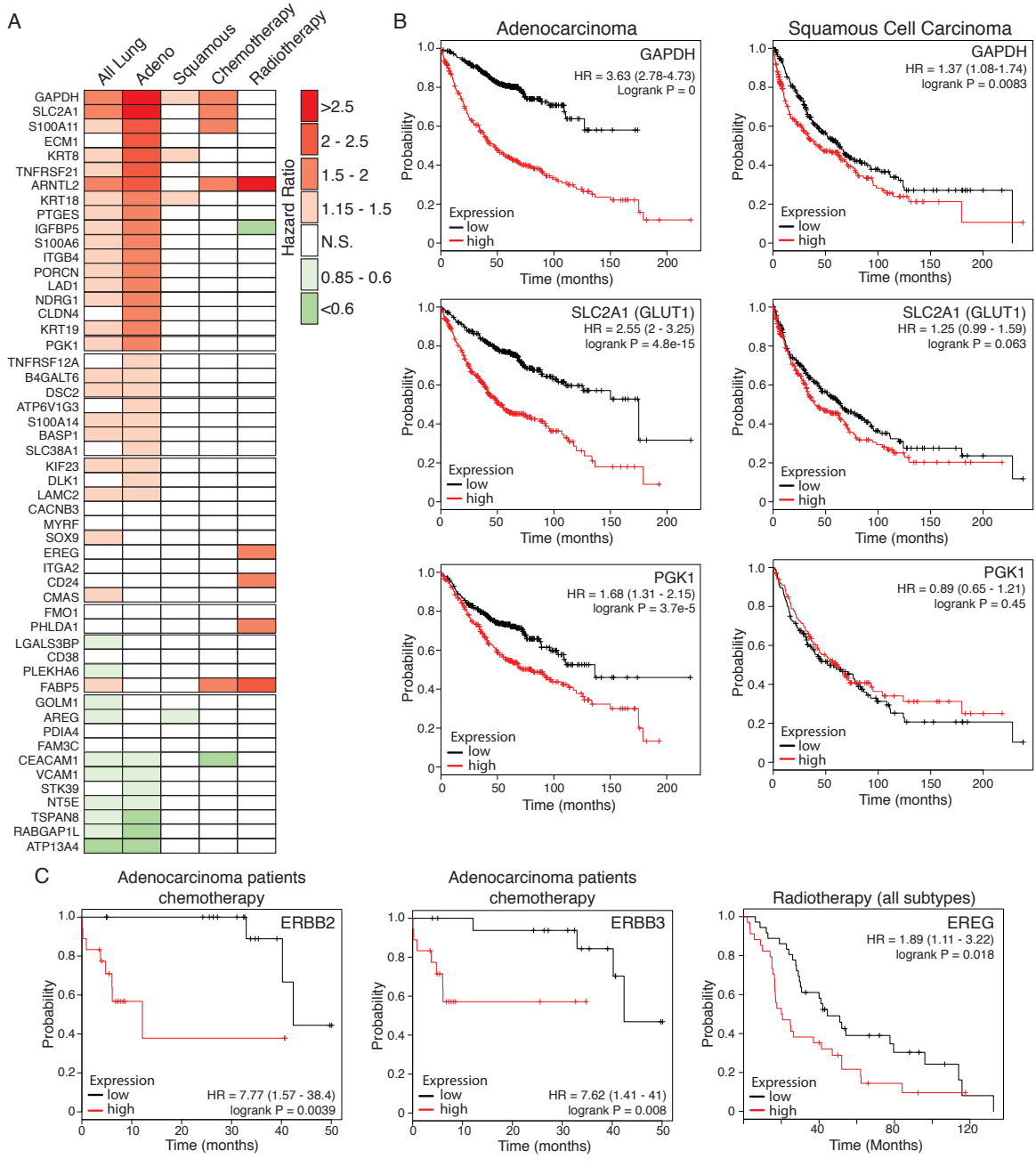

Figure 3: Relevance of the KM tumour progression signature for overall survival of human LuAd patients

A) *Hazard Ratios (HRs) of lung cancer patient overall survival associated with high expression of genes listed in Table 1, determined on the basis of above-versus-below median gene expression, using the KMplot survival analysis portal. Analysis shows statistically significant HRs for all lung patients included (N= 1926), those with Adenocarcinoma (Adeno; N=866), Squamous Cell Carcinoma (Squamous; N=675), and patients who received either Chemotherapy (N=178) or Radiotherapy (N=73). N.S. = Not statistically significant.* ***B)*** *Overall survival plots based on above (red lines) versus below (black lines) median expression of glycolysis pathway genes in human lung Adenocarcinoma (left panels) compared with lung Squamous Cell Carcinoma (right panels). HR = Hazard Ratio. 95% confidence intervals shown in parenthesis. For the Adenocarcinoma subtype, N = 866; for the Squamous subtype, N = 675.* ***C)*** *High expression of ERBB2 and ERBB3 is associated with worse outcome in human Adenocarcinoma patients receiving standard chemotherapy. Note that the low sample size available for this subgroup (N=36) require that the data be considered preliminary. Right panel: High expression of the ERBB ligand EREG is associated with worse outcome for lung cancer patients receiving radiotherapy (N=73). Low sample size precluded analysis of histological subtypes.*

ERBB3 is associated with resistance of Adenocarcinoma to chemotherapy, although these data should be interpreted with caution due to the low sample sizes available (Fig. 3C). The KM^2 mouse model thus exposes a number of genes that have meaningful impact on the overall survival and response to therapy of human lung Adenocarcinoma, attesting to its value as a model for this disease in humans.

3. Discussion

We previously identified a gene signature associated with sporadic progression to locally invasive Adenocarcinoma in a GEMM of lung cancer driven by endogenously expressed KRas^{G12D} combined with modestly overexpressed c-MYC [22]. Systematic analysis of each individual gene in this signature in multiple human NSCLC cell lines has identified conserved requirements for cell proliferation and identified a key role for WNT signalling in NSCLC cell migration. Crucially, analysis of human lung cancer patient survival data demonstrates that the KM^2 progression signature encompasses many genes that are significantly and specifically associated with overall survival of lung Adenocarcinoma patients. Intriguingly, several signature genes are associated with differential survival of patients treated with chemotherapy versus radiotherapy. Further validation of such genes may in future help guide selective treatment strategies for LuAd.

The KM^2 progression signature highlights the specific impact of the glycolytic cascade on patient survival: elevated expression of the glucose transporter *SLC2A1* and glycolytic enzymes *GAPDGH* and *PGK1* are associated with profoundly lower overall survival of Adenocarcinoma patients, with more modest associations in the Squamous Cell subtype. Increased glycolytic activity linked to tumour progression was also observed in an independent GEMM model and correlated with amplification of the active KRas^{G12D} allele [29]. As well as being processed for ATP consumption and macromolecular synthesis, much glucose uptake is diverted via the pentose phosphate and 1-carbon pathways for maintenance of cellular anti-oxidant capacity [30]. Although not included in our progression-associated gene signature, we found increased expression of many anti-oxidant genes as KM^2 tumour progress to invasive disease. The clinical relevance of anti-oxidant gene expression in LuAd is reflected loss of function mutations in KEAP1, which suppresses anti-oxidant

gene expression, in some 20% of cases. Genetic deletion of Keap1 or overexpression of its target, the anti-oxidant master regulatory transcription factor NRF2, accelerates KRas-driven LuAd in mice, suggesting that excessive oxidative stress limits tumour progression [31, 32]. Targeted suppression of the anti-oxidant pathway may thus expose lung tumours to excessive oxidative stress, leading to improved therapeutic outcomes [33].

Along the same lines, the KM^2 progression signature led us to identify an unexpected requirement for signalling through the ERBB family of receptor tyrosine kinases upstream of KRAS, despite the presence of the G12D activating mutation [22]. ERBB family proteins have proven to be far more amenable to pharmacological inhibition than KRAS itself and multiple ERBB inhibitors are approved for treatment of cancers expressing mutant or amplified ERBB isoforms. Indeed, we and others have demonstrated efficacy of broad-spectrum ERBB inhibitors against KRAS driven LuAd in vitro & vivo [22, 28, 34]. To this we now add patient survival data associated with overexpression of ERBB receptors and ligands, suggesting that elevated activity of this pathway may strongly influence responses to standard-of-care therapies. It is important to note that considerable redundancy exists within the ERBB network, between 4 receptors that can all homo- or hetero-dimerise upon binding of to up to 10 or more ligands. As such, broad specificity inhibition of all 4 RTKs maybe more desirable than selective inhibition of any one [35].

The KM^2 model thus recapitulates multiple salient molecular features with clear clinical relevance for human lung Adenocarcinoma. Data presented here represent analysis of the earliest detectable sporadic progression of KM^2 tumours to invasive heterogeneous disease, and it is worth noting that tumour heterogeneity increases along with emergence of metastases upon longer incubation [22]. The model thus allows incipient tumours to evolve sporadically, driven by emerging selective pressures rather than by the immediate consequence of transgene expression. Allowing autochthonous tumours to evolve in this manner likely exposes them to many of the same physiological barriers encountered by incipient human tumours, despite the complete absence of environmental toxins in the GEMM system, and this is reflected in the tumour progression signature. We believe that the KM^2 model is thus an excellent system for further investigation of lung tumour evolution and for pre-clinical evaluation of new therapeutic strategies.

4. Materials & Methods

4.1 Genetically Engineered Mice & Mouse Procedures: Procedures involving mice were performed in accordance with protocol numbers 55.2-2531.01-72/10 (University of Würzburg, Germany) and Home Office licence numbers 60/4183 & 70/7950 (CRUK BICR, UK). Rosa26$^{DM.lsl\text{-}MYC}$ mice were generated as previously described [22] using vectors described in [36]: Targeted insertion into the *Rosa26* locus was confirmed by Southern blotting and genotyping was performed using the following primers: A) CCC AAA GTC GCT CTG AGT TG (common); B) GCG AAG AGT TTG TCC TCA ACC (targeted locus); C) GGA GCG GGA GAA ATG GAT ATG A (wild-type locus). All genotyping was subsequently performed by Transnetyx Inc. *Lsl-KRas^{G12D}* [5] mice were obtained from the NCI mouse repository at Fredrick, MD, USA. Mice were maintained on a mixed FVBN/C57Bl6 background, housed on a 12hr light/dark cycle and fed and watered ad libitum. Both males and females were included in the study. Recombinant Adenovirus expressing Cre was purchased from

the University of Iowa gene therapy core facility. For Adeno-Cre installation, mice aged 8 weeks were sedated with a mixture of Domitor and Ketamine, injected IP. For most experiments $1x10^7$ pfu Adeno-CRE were administered intranasally using the calcium phosphate precipitation method, as described previously [17]. BrdU injection was performed at least 2hrs prior to sacrifice. All mice were sacrificed using a schedule 1 procedure. $Rosa26^{DM.lsl\text{-}MYC}$ mice are available upon request from D.J.M..

4.2 Immunohistochemistry and Tissue Analysis: Mouse tissues were perfused with zinc formalin overnight. 4µm paraffin sections were de-paraffinized and rehydrated: 3 x 5 minutes xylene, 2 minutes in each 2x100%; 2x95%; 2x70%; 1x50% ethanol; dH_2O. Peroxidase blocking was performed for 10 min in 3% H_2O_2 diluted in H_2O, followed by antigen retrieval in 10mM citrate buffer, pH 6, 10 minutes near boiling by microwave heating at low power. Non-specific antibody binding was blocked with up to 3% BSA or up to 5% normal goat serum for 1h at RT or overnight at 4^0C. Primary antibody incubation was performed overnight at 4^0C or 2h at 37^0C. Secondary biotinylated antibody was incubated 1h at room temperature and stain was developed with stable DAB (Invitrogen) followed by counterstaining with Gil 1 hematoxylin (Sigma MH216) and Scotts tap water substitute. The following antibodies were used at the indicated dilution: p-Erk (P44/42 MAPK phosphor-Thr202/Tyr204), Cell Signaling CS4370, BrdU, Serotec OBT0030CX, 1:250 or BD Biosciences 347580 1:200; Vectorlabs VECTASTAIN ABC kit; anti-Rabbit IgG, PK-4001 ECL; anti Rat, GE Healthcare NA935. Tumor burden was determined using Leica software as the % area of lung tissue occupied by tumors, measured on 3 Hematoxylin & Eosin (H&E) stained sections, separated by at least 100µm, from each of the indicated numbers of mice. Histological classification of tumours as Adenocarcinoma was determined by a clinical pathologist. Laser-capture and RNA-SEQ analysis were performed as previously described [22]. RNA-SEQ data are available from Arrayexpress: E-MTAB 6432.

4.3 Cell Culture and Related Assays: Established lung cancer cell lines (A549, H2009, H460) were validated in-house and grown in DMEM with 10% FBS & penn/strep. A focused de-convoluted library of 4 siRNAs targeting each of 51 selected gene products was purchased from Qiagen. For analysis of cell viability, cells were reverse transfected with individual siRNAs in 96-well plates at a density that yielded 70% confluence after 72hrs incubation when transfected with non-targeting control siRNA. Cells were transfected with each siRNA in technical quadruplicate, using either Lipofectamine 2000 or RNAi Max, after optimization of transfection for each cell line. 72hrs later, cells were washed with PBS, fixed with 4% PFA for 20 minutes, stained with DAPI and nuclei were counted using Columbus Image Analysis following image acquisition on an Operetta High Content Analyzer. Screening was performed in triplicate for each cell line. To measure effects on cell migration, cells were reverse transfected in 96-well plates at a density that yielded 100% confluence after 48hrs when transfected with non-targeting siRNA. After 48hrs, scratch wounds were made using a 96-point woundmaker tool. Scratch wounds were measured by Incucyte time-lapse video microscopy for up to 46hrs (A549) or 20hrs (H2009) after wounding. Cells were then fixed and DAPI-stained nuclei counted by Operetta. Migration screens were performed in triplicate for each cell line.

4.4 Statistical Analysis: Analysis was performed as previously reported [22]: Raw data obtained from quantitative Real Time PCR, FACS, siRNA screening and Incucyte assays were copied into Excel (Microsoft) spreadsheets. All Mean values, SD, and SEM values of biological replicates were calculated using the calculator function. Graphical representation of such data was also produced in Excel (Microsoft). Statistical significance for pairwise data was determined by the Student's T test. For multiple comparisons, ANOVA was used with a post-hoc Turkey test. * denotes $P<0.05$; ** denotes $P<0.01$; *** denotes $P<0.005$. For analysis of human survival data, univariate Cox regression plots to assess the association of individual genes with lung cancer patient overall survival were plotted using KMplot.com [26] with a median patient split. Where multiple probes were available for a single gene, the median Hazard Ratio is presented. P values from Logrank tests are provided.

Supplementary Materials: The following are available online at www.mdpi.com/XXXX: Figure S1: Generation of Rosa26$^{DM.lsl\text{-}MYC}$ mice. Figure S2: In vitro validation of KM^2 LuAd progression signature genes

Author Contributions: Experiments were performed and analyzed by S.N., B.K., T.M. & K.G.; Targeting vectors to generate Rosa26$^{DM.lsl\text{-}MYC}$ mice were designed and developed by D.J.M. and mice were generated by A.B. & B.N.; In vitro screening was performed by K.H. and analyzed by D.J. & E.S. of the CRUK Beatson Institute screening facility; RNA-SEQ was performed by W.C. and analyzed by A.H; Pathology was performed by C.D.; D.J.M. wrote the manuscript and all authors read and approved the manuscript for submission.

Funding: Funding for this work was provided by the British Lung Foundation (CSOBLF16-2), a Merck, Sharp & Dohme MINT collaborative agreement, European Commission Marie Curie mobility fellowships FP7-CIG-618448 (all to D.J.M.) & H2020-MCSA-705190 (B.K.), & Deutsche Krebshilfe grant 109220 (D.J.M.). T. M. was supported by BLF PhD studentship APHD13-5. Specialist equipment was funded by a generous donation from the M.J.M. Smith Trust (Glasgow). A.H., D.J., W.C. & E.S. and the Beatson Institute screening and sequencing facilities were funded via CRUK core grant A17196.

Acknowledgements: The authors wish to acknowledge all members of the Murphy lab past and present who contributed to the intellectual discourse over the project lifetime. Additional thanks to the CRUK Beatson Institute animal services unit and histology core facility.

Conflicts of Interest: The authors declare no conflicts of interest.

5. References

1. Kwon, M. C. & Berns, A. (2013) Mouse models for lung cancer, *Mol Oncol.* **7**, 165-77.
2. Kersten, K., de Visser, K. E., van Miltenburg, M. H. & Jonkers, J. (2017) Genetically engineered mouse models in oncology research and cancer medicine, *EMBO Mol Med.* **9**, 137-153.
3. Singh, M. & Johnson, L. (2006) Using genetically engineered mouse models of cancer to aid drug development: an industry perspective, *Clin Cancer Res.* **12**, 5312-28.
4. Singh, M., Murriel, C. L. & Johnson, L. (2012) Genetically engineered mouse models: closing the gap between preclinical data and trial outcomes, *Cancer Res.* **72**, 2695-700.
5. Jackson, E. L., Willis, N., Mercer, K., Bronson, R. T., Crowley, D., Montoya, R., Jacks, T. & Tuveson, D. A. (2001) Analysis of lung tumor initiation and progression using conditional expression of oncogenic K-ras, *Genes Dev.* **15**, 3243-8.
6. Tuveson, D. A., Shaw, A. T., Willis, N. A., Silver, D. P., Jackson, E. L., Chang, S., Mercer, K. L., Grochow, R., Hock, H., Crowley, D., Hingorani, S. R., Zaks, T., King, C., Jacobetz, M. A., Wang, L., Bronson, R. T., Orkin, S. H., DePinho, R. A. & Jacks, T. (2004) Endogenous oncogenic K-ras(G12D) stimulates proliferation and widespread neoplastic and developmental defects, *Cancer Cell.* **5**, 375-87.
7. Sarkisian, C. J., Keister, B. A., Stairs, D. B., Boxer, R. B., Moody, S. E. & Chodosh, L. A. (2007) Dose-dependent oncogene-induced senescence in vivo and its evasion during mammary tumorigenesis, *Nat Cell Biol.* **9**, 493-505.
8. Cancer Genome Atlas Research, N. (2014) Comprehensive molecular profiling of lung adenocarcinoma, *Nature.* **511**, 543-50.

9. Jackson, E. L., Olive, K. P., Tuveson, D. A., Bronson, R., Crowley, D., Brown, M. & Jacks, T. (2005) The differential effects of mutant p53 alleles on advanced murine lung cancer, *Cancer Res.* **65**, 10280-8.

10. Bardeesy, N., Aguirre, A. J., Chu, G. C., Cheng, K. H., Lopez, L. V., Hezel, A. F., Feng, B., Brennan, C., Weissleder, R., Mahmood, U., Hanahan, D., Redston, M. S., Chin, L. & Depinho, R. A. (2006) Both p16(Ink4a) and the p19(Arf)-p53 pathway constrain progression of pancreatic adenocarcinoma in the mouse, *Proc Natl Acad Sci U S A.* **103**, 5947-52.

11. Ji, H., Ramsey, M. R., Hayes, D. N., Fan, C., McNamara, K., Kozlowski, P., Torrice, C., Wu, M. C., Shimamura, T., Perera, S. A., Liang, M. C., Cai, D., Naumov, G. N., Bao, L., Contreras, C. M., Li, D., Chen, L., Krishnamurthy, J., Koivunen, J., Chirieac, L. R., Padera, R. F., Bronson, R. T., Lindeman, N. I., Christiani, D. C., Lin, X., Shapiro, G. I., Janne, P. A., Johnson, B. E., Meyerson, M., Kwiatkowski, D. J., Castrillon, D. H., Bardeesy, N., Sharpless, N. E. & Wong, K. K. (2007) LKB1 modulates lung cancer differentiation and metastasis, *Nature.* **448**, 807-10.

12. Evan, G. I., Wyllie, A. H., Gilbert, C. S., Littlewood, T. D., Land, H., Brooks, M., Waters, C. M., Penn, L. Z. & Hancock, D. C. (1992) Induction of apoptosis in fibroblasts by c-myc protein, *Cell.* **69**, 119-28.

13. Pelengaris, S., Khan, M. & Evan, G. I. (2002) Suppression of Myc-induced apoptosis in beta cells exposes multiple oncogenic properties of Myc and triggers carcinogenic progression, *Cell.* **109**, 321-34.

14. Dansen, T. B., Whitfield, J., Rostker, F., Brown-Swigart, L. & Evan, G. I. (2006) Specific requirement for Bax, not Bak, in Myc-induced apoptosis and tumor suppression in vivo, *J Biol Chem.* **281**, 10890-5.

15. Schmitt, C. A. & Lowe, S. W. (2002) Apoptosis and chemoresistance in transgenic cancer models, *J Mol Med (Berl).* **80**, 137-46.

16. Finch, A., Prescott, J., Shchors, K., Hunt, A., Soucek, L., Dansen, T. B., Swigart, L. B. & Evan, G. I. (2006) Bcl-xL gain of function and p19 ARF loss of function cooperate oncogenically with Myc in vivo by distinct mechanisms, *Cancer Cell.* **10**, 113-20.

17. Murphy, D. J., Junttila, M. R., Pouyet, L., Karnezis, A., Shchors, K., Bui, D. A., Brown-Swigart, L., Johnson, L. & Evan, G. I. (2008) Distinct thresholds govern Myc's biological output in vivo, *Cancer Cell.* **14**, 447-57.

18. Indra, A. K., Warot, X., Brocard, J., Bornert, J. M., Xiao, J. H., Chambon, P. & Metzger, D. (1999) Temporally-controlled site-specific mutagenesis in the basal layer of the epidermis: comparison of the recombinase activity of the tamoxifen-inducible Cre-ER(T) and Cre-ER(T2) recombinases, *Nucleic Acids Res.* **27**, 4324-7.

19. Muthalagu, N., Junttila, M. R., Wiese, K. E., Wolf, E., Morton, J., Bauer, B., Evan, G. I., Eilers, M. & Murphy, D. J. (2014) BIM is the primary mediator of MYC-induced apoptosis in multiple solid tissues, *Cell Rep.* **8**, 1347-53.

20. Ichim, G., Lopez, J., Ahmed, S. U., Muthalagu, N., Giampazolias, E., Delgado, M. E., Haller, M., Riley, J. S., Mason, S. M., Athineos, D., Parsons, M. J., van de Kooij, B., Bouchier-Hayes, L., Chalmers, A. J., Rooswinkel, R. W., Oberst, A., Blyth, K., Rehm, M., Murphy, D. J. & Tait, S. W. G. (2015) Limited mitochondrial permeabilization causes DNA damage and genomic instability in the absence of cell death, *Mol Cell.* **57**, 860-872.

21. Sanchez-Aguilera, A., Arranz, L., Martin-Perez, D., Garcia-Garcia, A., Stavropoulou, V., Kubovcakova, L., Isern, J., Martin-Salamanca, S., Langa, X., Skoda, R. C., Schwaller, J. & Mendez-Ferrer, S. (2014) Estrogen signaling selectively induces apoptosis of hematopoietic progenitors and myeloid neoplasms without harming steady-state hematopoiesis, *Cell Stem Cell.* **15**, 791-804.

22. Kruspig, B., Monteverde, T., Neidler, S., Hock, A., Kerr, E., Nixon, C., Clark, W., Hedley, A., Laing, S., Coffelt, S. B., Le Quesne, J., Dick, C., Vousden, K., Martins, C. P. & Murphy, D. J. (2018) The ERBB network facilitates KRAS-driven lung tumorigenesis, *Sci Transl Med.* **10**.

23. Bhattacharjee, A., Richards, W. G., Staunton, J., Li, C., Monti, S., Vasa, P., Ladd, C., Beheshti, J., Bueno, R., Gillette, M., Loda, M., Weber, G., Mark, E. J., Lander, E. S., Wong, W., Johnson, B. E., Golub, T. R., Sugarbaker, D. J. & Meyerson, M. (2001) Classification of human lung carcinomas by mRNA expression profiling reveals distinct adenocarcinoma subclasses, *Proc Natl Acad Sci U S A.* **98**, 13790-5.

24. Garber, M. E., Troyanskaya, O. G., Schluens, K., Petersen, S., Thaesler, Z., Pacyna-Gengelbach, M., van de Rijn, M., Rosen, G. D., Perou, C. M., Whyte, R. I., Altman, R. B., Brown, P. O., Botstein, D. & Petersen, I. (2001) Diversity of gene expression in adenocarcinoma of the lung, *Proc Natl Acad Sci U S A.* **98**, 13784-9.

25. Okayama, H., Kohno, T., Ishii, Y., Shimada, Y., Shiraishi, K., Iwakawa, R., Furuta, K., Tsuta, K., Shibata, T., Yamamoto, S., Watanabe, S., Sakamoto, H., Kumamoto, K., Takenoshita, S., Gotoh, N., Mizuno, H., Sarai, A., Kawano, S., Yamaguchi, R., Miyano, S. & Yokota, J. (2012) Identification of genes upregulated in ALK-positive and EGFR/KRAS/ALK-negative lung adenocarcinomas, *Cancer Res.* **72**, 100-11.

26. Gyorffy, B., Lanczky, A., Eklund, A. C., Denkert, C., Budczies, J., Li, Q. & Szallasi, Z. (2010) An online survival analysis tool to rapidly assess the effect of 22,277 genes on breast cancer prognosis using microarray data of 1,809 patients, *Breast cancer research and treatment.* **123**, 725-31.

27. de Geus-Oei, L. F., van der Heijden, H. F., Corstens, F. H. & Oyen, W. J. (2007) Predictive and prognostic value of FDG-PET in nonsmall-cell lung cancer: a systematic review, *Cancer.* **110**, 1654-64.

28. Moll, H. P., Pranz, K., Musteanu, M., Grabner, B., Hruschka, N., Mohrherr, J., Aigner, P., Stiedl, P., Brcic, L., Laszlo, V., Schramek, D., Moriggl, R., Eferl, R., Moldvay, J., Dezso, K., Lopez-Casas, P. P., Stoiber, D., Hidalgo, M., Penninger, J., Sibilia, M., Gyorffy, B., Barbacid, M., Dome, B., Popper, H. & Casanova, E. (2018) Afatinib restrains K-RAS-driven lung tumorigenesis, *Sci Transl Med.* **10**.

29. Kerr, E. M., Gaude, E., Turrell, F. K., Frezza, C. & Martins, C. P. (2016) Mutant Kras copy number defines metabolic reprogramming and therapeutic susceptibilities, *Nature.* **531**, 110-3.

30. Vander Heiden, M. G. & DeBerardinis, R. J. (2017) Understanding the Intersections between Metabolism and Cancer Biology, *Cell.* **168**, 657-669.

31. DeNicola, G. M., Karreth, F. A., Humpton, T. J., Gopinathan, A., Wei, C., Frese, K., Mangal, D., Yu, K. H., Yeo, C. J., Calhoun, E. S., Scrimieri, F., Winter, J. M., Hruban, R. H., Iacobuzio-Donahue, C., Kern, S. E., Blair, I. A. & Tuveson, D. A. (2011) Oncogene-induced Nrf2 transcription promotes ROS detoxification and tumorigenesis, *Nature.* **475**, 106-9.

32. Romero, R., Sayin, V. I., Davidson, S. M., Bauer, M. R., Singh, S. X., LeBoeuf, S. E., Karakousi, T. R., Ellis, D. C., Bhutkar, A., Sanchez-Rivera, F. J., Subbaraj, L., Martinez, B., Bronson, R. T., Prigge, J. R., Schmidt, E. E., Thomas, C. J., Goparaju, C., Davies, A., Dolgalev, I., Heguy, A., Allaj, V., Poirier, J. T., Moreira, A. L., Rudin, C. M., Pass, H. I., Vander Heiden, M. G., Jacks, T. & Papagiannakopoulos,

T. (2017) Keap1 loss promotes Kras-driven lung cancer and results in dependence on glutaminolysis, *Nat Med.* **23**, 1362-1368.

33. Port, J., Muthalagu, N., Raja, M., Ceteci, F., Monteverde, T., Kruspig, B., Hedley, A., Kalna, G., Lilla, S., Neilson, L., Brucoli, M., Gyuraszova, K., Tait-Mulder, J., Mezna, M., Svambaryte, S., Bryson, A., Sumpton, D., McVie, A., Nixon, C., Drysdale, M., Esumi, H., Murray, G. I., Sansom, O. J., Zanivan, S. R. & Murphy, D. J. (2018) Colorectal Tumors Require NUAK1 for Protection from Oxidative Stress, *Cancer Discov.* **8**, 632-647.

34. Sun, C., Hobor, S., Bertotti, A., Zecchin, D., Huang, S., Galimi, F., Cottino, F., Prahallad, A., Grernrum, W., Tzani, A., Schlicker, A., Wessels, L. F., Smit, E. F., Thunnissen, E., Halonen, P., Lieftink, C., Beijersbergen, R. L., Di Nicolantonio, F., Bardelli, A., Trusolino, L. & Bernards, R. (2014) Intrinsic resistance to MEK inhibition in KRAS mutant lung and colon cancer through transcriptional induction of ERBB3, *Cell Rep.* **7**, 86-93.

35. Mishra, R., Hanker, A. B. & Garrett, J. T. (2017) Genomic alterations of ERBB receptors in cancer: clinical implications, *Oncotarget.* **8**, 114371-114392.

36. Srinivas, S., Watanabe, T., Lin, C. S., William, C. M., Tanabe, Y., Jessell, T. M. & Costantini, F. (2001) Cre reporter strains produced by targeted insertion of EYFP and ECFP into the ROSA26 locus, *BMC Dev Biol.* **1**, 4.